




Article

# Surface Plasmon Enhancement of $\text{Eu}^{3+}$ Emission Intensity in $\text{LaPO}_4/\text{Ag}$ Nanoparticles

Sanja Kuzman, Jovana Periša, Vesna Đorđević , Ivana Zeković, Ivana Vukoje, Željka Antić \*   
and Miroslav D. Dramićanin 

VINČA Institute of Nuclear Sciences-National Institute of the Republic of Serbia, University of Belgrade, 11000 Belgrade, Serbia; sanjaculubrk@gmail.com (S.K.); jburojevic@vinca.rs (J.P.); vesipka@vinca.rs (V.Đ.); zekovicivana@gmail.com (I.Z.); ivanav@vinca.rs (I.V.); dramican@vinca.rs (M.D.D.)

\* Correspondence: zeljkaa@gmail.com

Received: 25 May 2020; Accepted: 3 July 2020; Published: 10 July 2020



**Abstract:** A promising way to improve the performance of luminescent materials is to combine them with noble metal nanoparticles. Herein, a set of silver/europium-doped lanthanum orthophosphate ( $\text{Ag}/\text{La}_{0.95}\text{Eu}_{0.05}\text{PO}_4$ ) nanostructures with different concentrations of silver nanoparticles were prepared and investigated. The presented overlap between the strongest europium ( $\text{Eu}^{3+}$ ) excitation line and the broad silver nanoparticle surface plasmon resonance makes the combination prospective for coupling. X-ray powder diffraction confirmed the monoclinic monazite structure. The transmission electron microscopy revealed particles with a rod-like shape and  $\sim 4$  aspect ratio. Photoluminescence spectra show characteristic  $\text{Eu}^{3+}$  ion red emission. One of the requirements for an enhanced luminescence effect is the precise control of the distance between the noble metal nanoparticles and the emitter ion. The distance is indirectly varied throughout the change of Ag nanoparticle concentration in the  $\text{La}_{0.95}\text{Eu}_{0.05}\text{PO}_4$  host. The emission intensity increases with the increase in Ag nanoparticles up to 0.6 mol %, after which the luminescence decreases due to the nanoparticles' close packing and aggregation leading to the displacement of  $\text{La}_{0.95}\text{Eu}_{0.05}\text{PO}_4$  from the vicinity of the metal particles and reabsorption of the emitted light. The emission intensity of  $\text{La}_{0.95}\text{Eu}_{0.05}\text{PO}_4$  increases more than three times when the  $\text{Eu}^{3+}$  excitation is supported by the localized surface plasmon resonance in the  $\text{Ag}/\text{La}_{0.95}\text{Eu}_{0.05}\text{PO}_4$  nanostructures.

**Keywords:** inorganic materials; luminescence; optical properties; plasmonics

## 1. Introduction

Advanced materials are crucial for social and economic development, with applications in industries aimed to meet the challenges of renewable and clean energy, climate changes, national security, as well as human health and welfare. Therefore, the development and exploitation of innovative materials is critical in achieving global competitiveness in the 21st century. To meet, among others, demands for better physical and chemical sensors, brighter phosphors, or biocompatible drug-delivery molecules, material scientists are searching for new molecular combinations and structures [1–4].

The design and preparation of phosphors, inorganic materials activated by lanthanide ( $\text{Ln}^{3+}$ ) or transition metal (TM) ions, with different particle size and/or distinctive morphology is a challenging task that has attracted researchers' attention. Phosphors are used in a variety of applications, such as displays, lighting, optical sensing (physical and chemical), catalysis, and medicine, just to mention a few [5–7]. Phosphor's luminescent properties depend on the characteristics of the optically active ion and its local environment provided by the host lattice. In recent years, the lanthanum orthophosphate ( $\text{LaPO}_4$ ), non-toxic, biocompatible, thermally, chemically, and photo-stable material has been recognized

as an excellent choice for rare-earth ion doping [8–12]. Due to the similar ionic radii and charge, lanthanum ion ( $\text{La}^{3+}$ ) can be easily replaced with different rare-earth ( $\text{RE}^{3+}$ ) ions (e.g.,  $\text{Eu}^{3+}$ ,  $\text{Dy}^{3+}$ ,  $\text{Sm}^{3+}$ ) at a wide range of concentrations without significantly affecting the lattice structure [13].

The optical properties of luminescent materials can be improved by different approaches, such as by the optimization of the particle size and distribution, morphology, and crystal defects. Moreover, the modification of the local structure based on strategies such as the control of the doping level, cationic, anionic and cationic/anionic substitution, crystal-site engineering, and the mixing of nanophases are also promising routes [14]. To date, to improve and optimize the luminescence properties of  $\text{LaPO}_4$ -based phosphors, studies have focused on changing the particle size and shape, designing core-shell structures, surface modification, and co-doping with alkali metals [15–22]. However,  $\text{Ln}^{3+}$  activated phosphors suffer from the very low absorption in the near-UV and visible spectral regions due to quantum mechanically forbidden  $f$ - $f$  electronic transitions. For this reason, they cannot be used for the blue or near-UV excited LEDs unless their luminescence is not appropriately sensitized by co-dopants (for example,  $\text{Bi}^{3+}$ ,  $\text{Ce}^{3+}$ ), dyes, or plasmon particles. Collective oscillations of surface electrons in noble metal nanoparticles (plasmons) resonantly interact with the incident or emitting radiation, causing an increase in the light absorption cross-section and the radiative rate of an adjacent emitter. Thus, the brightness of  $\text{Ln}^{3+}$  and TM ion-activated phosphors may be increased through more effective light absorption when they are located in the vicinity of plasmon particles, for example noble metal clusters. Among different plasmonic structures, Ag nanoparticles are particularly useful for the phosphors' research because their plasmon occurs around 430 nm that is suitable for sensitizing most of the  $\text{Ln}^{3+}$  activators. To date, there is a number of reports on the phosphor/Ag nanoparticle (NP) systems as a promising combination for the emission enhancement [23–32]. However, there are only a few reports on the Ag plasmon-enhanced emission of  $\text{LaPO}_4$ -based phosphors. Li et al. investigated the enhancement of luminescent properties in inverse opal and silica-coated inverse opal  $\text{LaPO}_4:\text{Eu}^{3+}$  structures after the addition of Ag nanoparticles [33,34]. For silica-coated inverse opal structures, they reported the enhancement factor of  $\sim 7$ .

The aim of this work was to investigate how co-doping with silver nanoparticles affects the luminescence properties of the  $\text{La}_{0.95}\text{Eu}_{0.05}\text{PO}_4$  phosphor. A simple hydrothermal method was used for the preparation of  $\text{Ag}/\text{La}_{0.95}\text{Eu}_{0.05}\text{PO}_4$  nanostructures with different silver nanoparticles concentrations. Lanthanum orthophosphate and hydrothermal synthesis were chosen due to the low crystallization and reaction temperature which prevents silver nanoparticles from melting and agglomeration [23]. Structural, morphological, and optical properties were reported and discussed. The effect of silver nanoparticles on the luminescence properties of  $\text{La}_{0.95}\text{Eu}_{0.05}\text{PO}_4$  is elaborated in terms of Ag NPs optimal concentration and luminescence enhancement factor.

## 2. Materials and Methods

### 2.1. Synthesis of $\text{Ag}/\text{La}_{0.95}\text{Eu}_{0.05}\text{PO}_4$ Nanostructures

A set of six samples was prepared by the conventional hydrothermal synthesis. Five samples were prepared by using silver colloids of different concentrations ( $1 \times 10^{-4}$  M;  $2 \times 10^{-4}$  M;  $1 \times 10^{-3}$  M;  $2 \times 10^{-3}$  M;  $3 \times 10^{-3}$  M) as a medium, while one sample was prepared in water (see Figure 1 for the sample's names and Ag NPs mol %). The mole percentages (mol %) of Ag NPs in the samples were calculated relative to the overall content in the  $\text{Ag}/\text{La}_{0.95}\text{Eu}_{0.05}\text{PO}_4$  nanostructures. According to our previous results [13], there is no concentration quenching in  $\text{RE}^{3+}$ -doped  $\text{LaPO}_4$  NPs and the emission intensity increases with an increase in  $\text{RE}^{3+}$  dopant concentration up to the full substitution of  $\text{La}^{3+}$  with  $\text{RE}^{3+}$ . We chose the  $\text{La}_{0.95}\text{Eu}_{0.05}\text{PO}_4$  system where the  $\text{Eu}^{3+}$  emission is strong enough so that the effect of Ag NPs on the luminescence efficiency can be clearly observed.

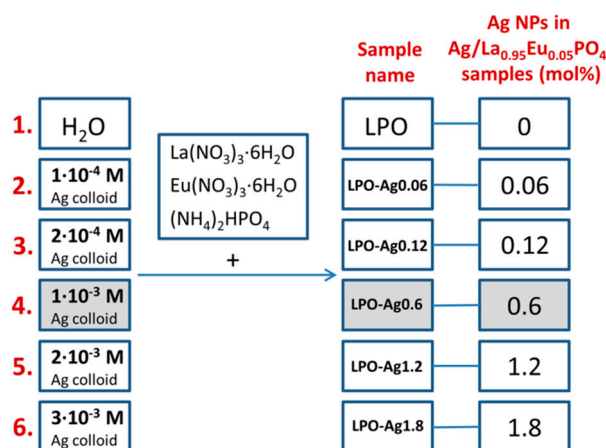


**Figure 1.** Marking of the La<sub>0.95</sub>Eu<sub>0.05</sub>PO<sub>4</sub> (LPO) samples with different concentrations of Ag nanoparticles (NPs).

**Synthesis of silver colloid:** An appropriate amount of silver nitrate (AgNO<sub>3</sub>, Merck) was dissolved in the water previously purged with argon for 30 min. The reducing sodium borohydride (NaBH<sub>4</sub>) agent was added to the solution by vigorous stirring. A large excess of NaBH<sub>4</sub> was required to reduce the silver ions and to stabilize the formed silver nanoparticles. The obtained colloids were left in an argon atmosphere for an additional 30 minutes. The concentrations of obtained silver colloids were: 1 × 10<sup>-4</sup> M; 2 × 10<sup>-4</sup> M; 1 × 10<sup>-3</sup> M; 2 × 10<sup>-3</sup> M and 3 × 10<sup>-3</sup> M, and they were used without any further purification.

**Synthesis of Ag/La<sub>0.95</sub>Eu<sub>0.05</sub>PO<sub>4</sub> nanostructures:** In the first step, the stoichiometric quantities of lanthanum(III) nitrate hexahydrate (La(NO<sub>3</sub>)<sub>3</sub>·6H<sub>2</sub>O, Alfa Aesar, 99.9%), europium(III) nitrate pentahydrate (Eu(NO<sub>3</sub>)<sub>3</sub>·6H<sub>2</sub>O, Alfa Aesar, 99.9%) and diammonium hydrogen phosphate ((NH<sub>4</sub>)<sub>2</sub>HPO<sub>4</sub>, Alfa Aesar, 98.0%) were dissolved in an appropriate amount of water/silver colloid. The resulting solutions (20 mL) were transferred into a 50 mL Teflon-lined Stainless Steel Autoclave and kept at 140 °C for 30 h, followed by natural cooling to room temperature. Obtained white precipitates were washed with distilled water and ethanol and dried at 40 °C.

## 2.2. Instruments and Measurements

X-ray diffraction (XRD) measurements were performed using the Rigaku SmartLab diffractometer, Rigaku Corporation, Tokyo, Japan. Diffraction data were recorded in a 2θ range from 10° to 90°, counting 0.1°/min in 0.02° steps. Transmission electron microscopy was performed on the FEI TECNAI G2 X-TWIN microscope. Diffuse spectral reflectance measurements were performed on the Thermo Evolution 600 spectrometer equipped with an intergrading sphere, using BaSO<sub>4</sub> as a blank. The photoluminescent emission spectra were collected using a Fluorolog-3 Model FL3-221 spectrofluorometer system (Horiba-Jobin-Yvon) under continuous excitation using a 450W xenon lamp (λ<sub>ex</sub> = 393 nm). The photoluminescent excitation spectra were recorded while monitoring emission at λ<sub>em</sub> = 611 nm.

## 3. Results and Discussion

### 3.1. Structural Analysis

X-ray powder diffraction patterns of the representative LPO and two Ag/La<sub>0.95</sub>Eu<sub>0.05</sub>PO<sub>4</sub> (LPO–Ag0.6 and LPO–Ag1.8) samples confirmed the monoclinic monazite structure with space group P 121/n 1(14) (see Figure 2a, all diffraction peaks are indexed according to the COD card no. 9001647). The absence of impurity phases indicates that the dopant Eu<sup>3+</sup> ions are successfully incorporated into the LaPO<sub>4</sub> matrix due to the equal valence (+3) and similar ionic radii between the Eu<sup>3+</sup> (*a* = 0.112 nm) and La<sup>3+</sup> ions (*a* = 0.122 nm) [35]. In this crystal structure, the lanthanide ions

are coordinated with nine oxygen atoms forming polyhedrons ( $\text{LaO}_9$ ) that share a corner with  $\text{PO}_4$  tetrahedra in which all four P–O bonds are equivalent (Figure 2b,c) [13,36]. The average crystallite size of ~6 nm was determined using built-in software and was similar for all the samples.

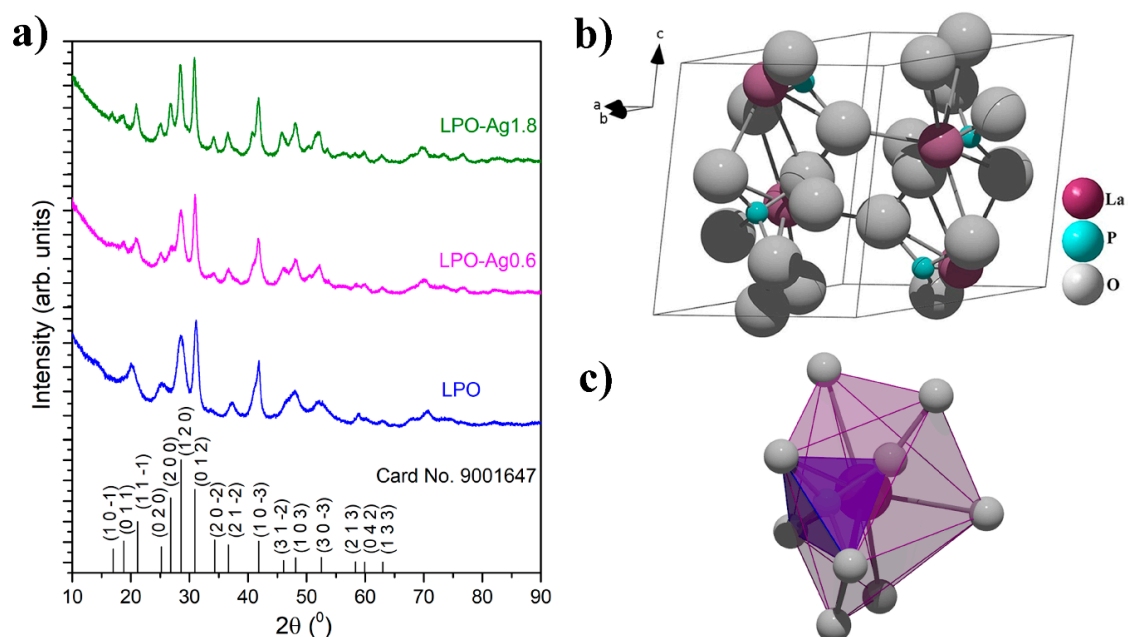


**Figure 2.** (a) XRD patterns of the representative LPO, LPO–Ag0.6, and LPO–Ag1.8 samples. The diffraction peaks are indexed according to the Crystallography Open Database - COD card No. 9001647. Lanthanum phosphate ( $\text{LaPO}_4$ ); (b) unit cell; and (c) coordination polyhedron around  $\text{La}^{3+}$ .

### 3.2. Microstructural Characterization

Transmission electron microscopy images (Figure 3a–c) of the representative LPO–Ag0.6 sample show particles with a rod-like shape, expected for the given monoclinic crystal system. Furthermore, the TEM images reveal an aggregation tendency also found in higher condensed La-based phosphates [37]. An average length/diameter aspect ratio was calculated and found to be around 4 (Figure 3d–f). According to the literature [38,39], when synthesized under alkaline conditions ( $\text{pH} > 7$ ) the particles are sphere-like. On the other hand, when synthesized under acidic conditions ( $\text{pH} < 7$ ), the particles become rod-like with a different length/diameter ratio corresponding to the different pH values. In a strongly acidic solution, rod-like morphology becomes fiber-like having a width of 5–20 nm and a length of several micrometers. Herein, the prepared mildly acidic precursor solutions ( $\text{pH} \sim 5$ ) yield to, as expected, rod-like particles with ~4 aspect ratio.

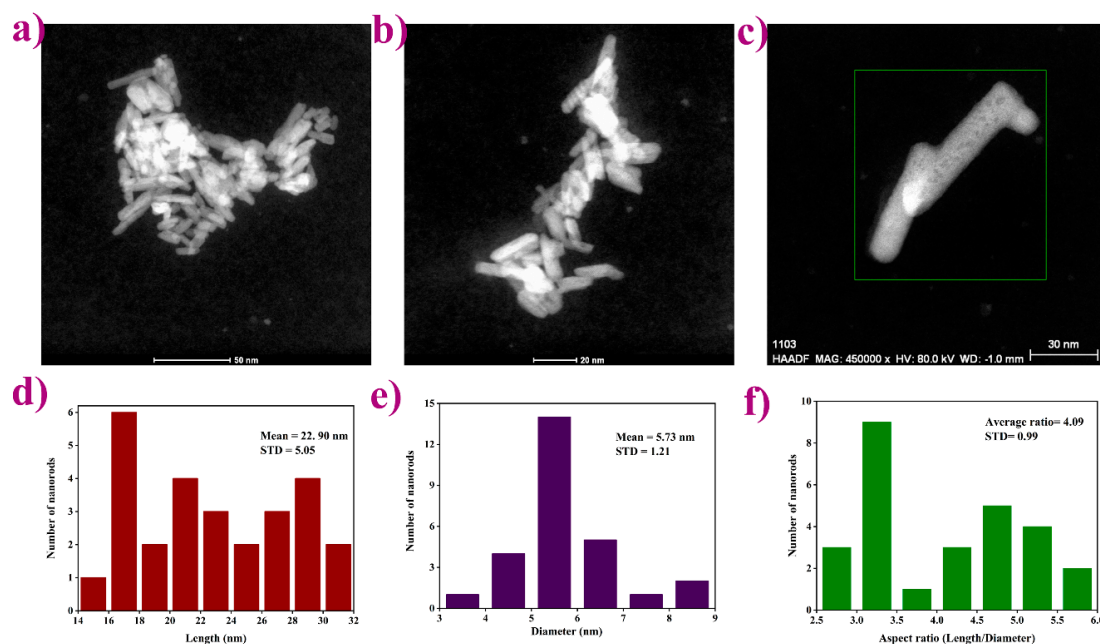


**Figure 3.** Transmission electron microscopy images showing: (a–c) anisotropic rod-like shape particles with an aggregation tendency; (d–f) average length/diameter/aspect ratio histograms.

### 3.3. Diffuse Reflectance

Figure 4 shows the diffuse reflectance spectra of the representative LPO and LPO–Ag0.6 samples. The sample with the Ag NPs clearly shows a typical broad band centred at 430 nm originating from the Ag surface plasmon resonance [40,41]. On the other hand, the sample without Ag NPs shows only weak bands that correspond to the  $\text{Eu}^{3+}$  transitions with the most distinguished  ${}^7\text{F}_0 \rightarrow {}^5\text{L}_6$  absorption placed  $\sim 393$  nm. An enlarged inset clearly shows how Ag plasmon absorption overlaps the  ${}^7\text{F}_0 \rightarrow {}^5\text{L}_6$  absorption band of the  $\text{Eu}^{3+}$  ion [42,43].

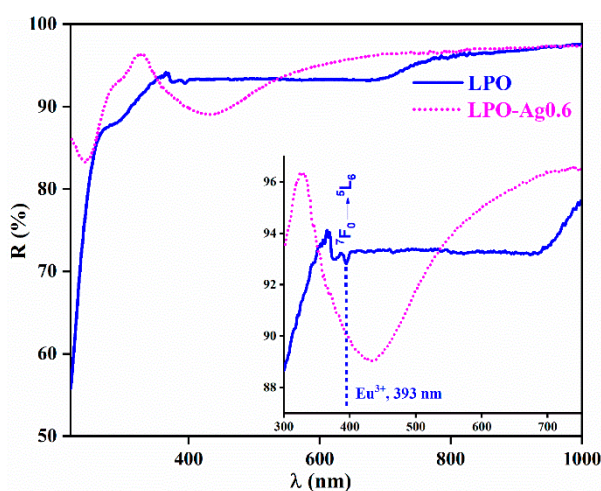


**Figure 4.** Diffuse reflectance spectra of the representative LPO (blue solid line) and LPO–Ag0.6 (pink-dotted line) sample. Inset: the dip in the reflection spectrum of the LPO–Ag0.6 sample centred at 430 nm is due to Ag plasmon absorption and it overlaps with the  ${}^7\text{F}_0 \rightarrow {}^5\text{L}_6$  absorption band of  $\text{Eu}^{3+}$ .

### 3.4. Photoluminescence Measurements

Figure 5 presents the UV–VIS absorption spectrum of the representative Ag colloid ( $1 \times 10^{-3}$  M) together with the theoretical extinction efficiency curve for 6 nm spherical Ag particles in water and the excitation spectrum of the representative LPO–Ag0.6 sample. The UV–VIS absorption spectra of

all silver colloids used for the synthesis ( $1 \times 10^{-4}$  M;  $2 \times 10^{-4}$  M;  $1 \times 10^{-3}$  M;  $2 \times 10^{-3}$  M;  $3 \times 10^{-3}$  M) are given in the Supporting Material as Figure S1. The excitation spectrum of the LPO–Ag0.6 sample ( $\lambda_{em} = 611\text{nm}$ ) consists of several sharp lines that correspond to the transitions within the  $4f^6$  configuration of  $\text{Eu}^{3+}$  ions. The strongest  $\text{Eu}^{3+}$  line in the LPO–Ag0.6 excitation spectrum ( ${}^7F_0 \rightarrow {}^5L_6$  at 393 nm) overlaps with the silver nanoparticles' plasmon resonance, making this combination prospective for coupling. The incident light wave resonates with oscillations of the surface electron plasma in the Ag NPs at a certain resonance frequency/wavelength. The light-induced, so-called surface plasmon, electric field spreads outside the Ag NPs and influences the neighbouring  $\text{Eu}^{3+}$  ions by increasing their light absorption. Thus, the  $\text{Eu}^{3+}$  ions will absorb more and therefore emit more light. In that way, by the incorporation of Ag NPs into the LPO host, the intensity of  $\text{Eu}^{3+}$  emission could be enhanced [23].

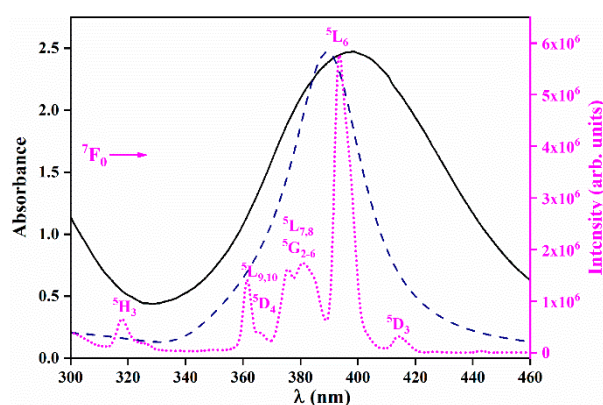


**Figure 5.** Ag NPs' plasmonic absorption (black solid line) and the theoretical extinction efficiency curve for the 6 nm spherical Ag particles in water (blue dashed line), overlapping with the excitation spectrum of the LPO–Ag0.6 representative sample ( $\lambda_{em} = 611\text{nm}$ , pink dotted line).

Figure 6a shows the photoluminescence spectra of all six samples, the LPO and the five samples with different concentrations of Ag NPs. Five characteristic  $\text{Eu}^{3+}$  emission bands associated with  ${}^5D_0 \rightarrow {}^7F_J$  ( $J = 0, 1, 2, 3, 4$ ) spin forbidden  $f-f$  transitions, are visible around 578, 587, 611, 652, and 698 nm, respectively. It is well known that the  ${}^5D_0 \rightarrow {}^7F_1$  transition of  $\text{Eu}^{3+}$  ion is the parity-allowed magnetic dipole transition ( $\Delta J = 1$ ) and its intensity does not vary with the host. On the other hand, red  ${}^5D_0 \rightarrow {}^7F_2$  electric dipole transition ( $\Delta J = 2$ ) is highly sensitive to the local environment, and its intensity decreases with an increase in the symmetry of the crystal field around the europium ion. In the given structure, the  $\text{Eu}^{3+}$  ion replaces  $\text{La}^{3+}$  in the non-centrosymmetric C1 crystallographic site. It is generally acknowledged that the observation of the dominant  ${}^5D_0 \rightarrow {}^7F_2$  line and completely forbidden  ${}^5D_0 \rightarrow {}^7F_0$  transition indicates that  $\text{Eu}^{3+}$  ion is located in a structural site without an inversion centre (such as C1) [42,43]. This is in agreement with the observed photoluminescence spectra where the red emission arising from the  ${}^5D_0 \rightarrow {}^7F_2$  transition is more intense compared to the  ${}^5D_0 \rightarrow {}^7F_1$  emission.

One of the conditions for enhanced luminescence effect is the precise control of a distance between the plasmon particles and the emitter. Here, the distance is indirectly varied by changing the Ag nanoparticle's concentration in the  $\text{La}_{0.95}\text{Eu}_{0.05}\text{PO}_4$  host. Figure 6b shows the normalized integrated area of the photoluminescent emission spectra as a function of Ag NPs mol % in nanostructures. The emission intensity increases up to 0.6 mol % of Ag NPs while higher Ag concentrations cause emission intensity decrease. When the concentration of Ag NPs is  $\leq 0.6$  mol %, phosphor particles are located in the vicinity of plasmon particles which results in the increase in emission intensity due to more effective light absorption. The optimal Ag NP concentration is 0.6 mol % and it results in the ~3 emission enhancement factor (distribution of the light-induced electric field near Ag nanoparticles calculated by the means of the discrete dipole approximation, given and discussed in the Supporting Material as Figure S2). On the other hand, the high Ag NP concentrations ( $>0.6$  mol %) cause the close packing and aggregation of the plasmon particles leading to:

- (i) the displacement of  $\text{La}_{0.95}\text{Eu}_{0.05}\text{PO}_4$  phosphor particles from the vicinity of the metal particles and consequently a luminescence efficiency decrease [20];
- (ii) the reabsorption of emitted light, due to the electromagnetic coupling between the neighbouring particles in the aggregates. Quinten et al. reported that the Ag aggregate spectra clearly show single-particle resonance splitting into new resonances, most of which contribute at longer wavelengths ( $\sim 500\text{--}600$  nm) than the resonance wavelength of the single particle ( $\sim 400$  nm). Thus, the strongest  $\text{Eu}^{3+}$  excitation line ( $\sim 393$  nm) does not overlap efficiently with the silver nanoparticles' plasmon resonance [44].

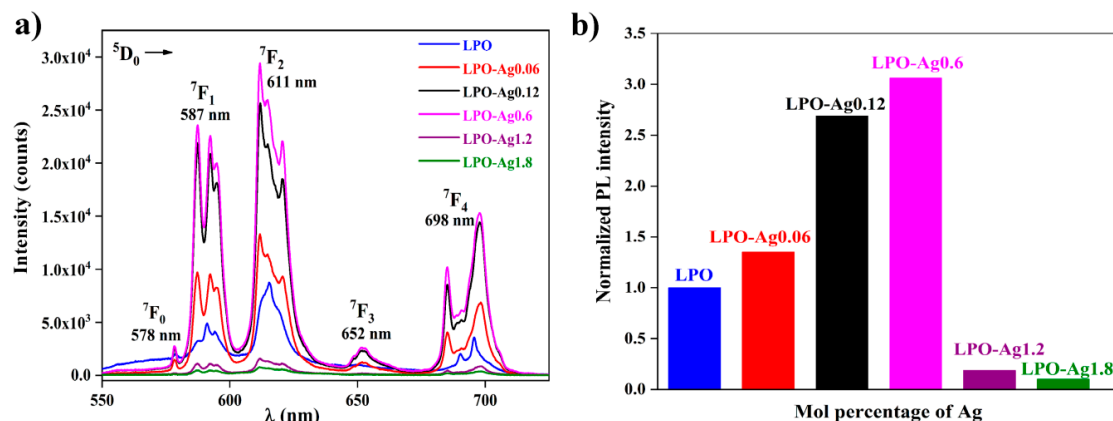


**Figure 6.** (a) Photoluminescence emission spectra of the LPO and Ag/ $\text{La}_{0.95}\text{Eu}_{0.05}\text{PO}_4$  nanostructures; (b) the normalized photoluminescent (PL) intensity as a function of the Ag NP concentration in the LPO and Ag/ $\text{La}_{0.95}\text{Eu}_{0.05}\text{PO}_4$  nanostructures showing the maximum enhancement factor  $\sim 3$ .

#### 4. Conclusions

The brightness of phosphors can be increased due to stronger light absorption when phosphor particles are located in the vicinity of plasmon particles, for example noble metal clusters. Herein, we showed that the surface plasmon resonance facilitated the enhancement of the  $\text{Eu}^{3+}$ -doped  $\text{LaPO}_4$  emission intensity by the addition of Ag nanoparticles. One of the conditions for the enhancement of the phosphors' emission intensity was the precise control of the distance between the plasmon particles and the phosphor. The distance is indirectly varied by the Ag NPs concentration in the structure. When the Ag NPs concentration is low, i.e., when there is a small number of Ag NPs, the distance between the Ag and phosphor particles is long. With the Ag NPs concentration increase, the distance becomes shorter, reaching the optimum at 0.6 mol % Ag and resulting in a three times larger value than the initial photoluminescent intensity. One could expect that with the further increase in concentration (and number of NPs), the distance would be even shorter, leading to further photoluminescent intensity enhancement. However, that is not the case due to the close packing and aggregation of the plasmon particles which causes both the reabsorption of emitted light and the displacement of the  $\text{La}_{0.95}\text{Eu}_{0.05}\text{PO}_4$  phosphor particles from the vicinity of the metal particles. The distance between the phosphor particles and the Ag NPs can also be adjusted by coating phosphor particles with a different thickness  $\text{SiO}_2$  shell, which will be a subject of our future work.

**Supplementary Materials:** The following are available online at <http://www.mdpi.com/1996-1944/13/14/3071/s1>, Figure S1: UV-VIS absorption spectra of the different concentrations of silver colloids, Figure S2: Distribution of the square of the electric field amplitude  $(E/E_0)^2$  for 6 nm spherical Ag nanoparticles (NPs) in (a) water and in (b)  $\text{La}_{0.95}\text{Eu}_{0.05}\text{PO}_4$  (LPO).

**Author Contributions:** Conceptualization, M.D.D.; methodology, Ž.A. and M.D.D.; data curation, V.Đ.; formal analysis, S.K., J.P., Ž.A.; investigation, S.K., I.Z., I.V.; writing—original draft preparation, S.K. and Ž.A.; visualization, S.K., V.Đ., J.P. and Ž.A.; writing—review and editing Ž.A. and M.D.D. All authors have read and agreed to the published version of the manuscript.

**Funding:** The authors acknowledge funding from the European Union's Horizon 2020 FET Open Program under grant agreement No. 801305, and from the Ministry of Education, Science and Technological Development of the Republic of Serbia.

**Conflicts of Interest:** The authors declare no conflict of interest.

## References

1. Materials Genome Initiative. Available online: <https://www.mgi.gov/> (accessed on 22 May 2020).
2. Advanced Materials and Applications: Tackling New R&D and Engineering Challenges. Elsevier: Amsterdam, Netherlands. Available online: [https://www.elsevier.com/\\_data/assets/pdf\\_file/0018/120942/R-D-Solutions\\_CHEM\\_Ebook\\_Advanced-Materials\\_DIGITAL.pdf](https://www.elsevier.com/_data/assets/pdf_file/0018/120942/R-D-Solutions_CHEM_Ebook_Advanced-Materials_DIGITAL.pdf) (accessed on 25 June 2020).
3. Kar, S. An overview of recent advances in application of some inorganic materials-biological and technological perspectives. *J. Biotechnol. Biomater.* **2016**, *6*, 7. [[CrossRef](#)]
4. Shubha, G.N.; Tejaswini, M.L.; Lakshmi, K.P. Advanced material for newer applications. *Mater. Today Proc.* **2018**, *5*, 2541–2546. [[CrossRef](#)]
5. Dramićanin, D.M. *Luminescence Thermometry, Methods, Materials, and Applications*, 1st ed.; Elsevier: Cambridge, UK, 2018. [[CrossRef](#)]
6. Cao, G. *Nanostructures & Nanomaterials Synthesis, Properties & Applications*, 2nd ed.; Imperial College Press: London, UK, 2011. [[CrossRef](#)]
7. Blasse, G.; Grabmaier, B.C. *Luminescent Materials*, 1st ed.; Springer-Verlag: Berlin/Heidelberg, Germany, 1994. [[CrossRef](#)]
8. Shaik, N.P.; Poornachandra, R.N.V.; Murthy, K.V.R. Photoluminescence properties of Eu<sup>3+</sup>, Ce<sup>3+</sup> doped LaPO<sub>4</sub> phosphors. *Adv. Mater. Lett.* **2014**, *5*, 722–727. [[CrossRef](#)]
9. Runowski, M.; Grzyb, T.; Zep, A.; Krzyczkowska, P.; Gorecka, E.; Giersig, M.; Lis, S. Eu<sup>3+</sup> and Tb<sup>3+</sup> doped LaPO<sub>4</sub> nanorods, modified with luminescent organic compound, exhibiting tunable multicolour emission. *Rsc. Adv.* **2014**, *86*, 46305–46312. [[CrossRef](#)]
10. Malyy, T.S.; Vistovskyy, V.V.; Khapko, Z.A.; Pushak, A.S.; Mitina, N.E.; Zaichenko, A.S.; Gektin, A.V.; Voloshinovskii, A.S. Recombination luminescence of LaPO<sub>4</sub>-Eu and LaPO<sub>4</sub>-Pr nanoparticles. *J. Appl. Phys.* **2013**, *113*, 224305. [[CrossRef](#)]
11. Loc, D.X.; Chi, T.T.K.; Huong, T.T.; Anh, T.K.; Streck, W.; Minch, L.Q. Synthesis and characterization of core/shell structured nanophosphors CePO<sub>4</sub>:Tb@LaPO<sub>4</sub> by solvothermal method. *J. Rare Earths* **2011**, *29*, 1147–1151. [[CrossRef](#)]
12. Trejgis, K.; Maciejewska, K.; Bednarkiewicz, A.; Marciniak, L. Near infrared-to-near infrared excited-state absorption in LaPO<sub>4</sub>:Nd<sup>3+</sup> nanoparticles for luminescent nanothermometry. *ACS Appl. Nano Mater.* **2020**, *3*, 4818–4825. [[CrossRef](#)]
13. Gavrilović, T.; Periša, J.; Papan, J.; Vuković, K.; Smits, K.; Jovanović, J.D.; Dramićanin, D.M. Particle size effects on the structure and emission of Eu<sup>3+</sup>:LaPO<sub>4</sub> and EuPO<sub>4</sub> phosphors. *J. Lumin.* **2018**, *195*, 420–429. [[CrossRef](#)]
14. Lin, Y.-C.; Karlsson, M.; Bettinelli, M. Inorganic phosphor materials for lighting. *Top. Curr. Chem. (Z)* **2016**, *374*. [[CrossRef](#)]
15. Li, J.; Yang, Z.; Shao, B.; Yang, J.; Wang, Y.; Qiu, J.; Song, Z.; Yang, Y. Preparation and photoluminescence enhancement of silica-coated LaPO<sub>4</sub>:Eu<sup>3+</sup> three dimensional ordered macroporous films. *Ceram. Int.* **2015**, *41*, 8109–8113. [[CrossRef](#)]
16. Dorman, J.A.; Choi, J.H.; Kuzmanich, G.; Chang, J.P. High-quality white light using core-shell RE<sup>3+</sup>:LaPO<sub>4</sub> (RE = Eu, Tb, Dy, Ce) phosphors. *J. Phys. Chem. C* **2012**, *116*, 12854–12860. [[CrossRef](#)]
17. Van Hest, J.J.H.A.; Blab, A.G.; Gerritsen, H.C.; de Mello Donegá, C.; Meijerink, A. Probing the influence of disorder on lanthanide luminescence using Eu-doped LaPO<sub>4</sub> nanoparticles. *J. Phys. Chem. C* **2017**, *121*, 19373–19382. [[CrossRef](#)] [[PubMed](#)]
18. Stouwdam, J.W.; Van Veggel, F.C.J.M. Improvement in the luminescence properties and processability of LaF<sub>3</sub>/Ln and LaPO<sub>4</sub>/Ln nanoparticles by surface modification. *Langmuir* **2004**, *20*, 11763–11771. [[CrossRef](#)] [[PubMed](#)]
19. Yu, L.; Song, H.; Lu, S.; Liu, Z.; Yang, L.; Kong, X. Luminescent properties of LaPO<sub>4</sub>:Eu nanoparticles and nanowires. *J. Phys. Chem. B* **2004**, *108*, 16697–16702. [[CrossRef](#)]



20. Ansari, A.A. Silica-modified luminescent LaPO<sub>4</sub>:Eu@LaPO<sub>4</sub>@SiO<sub>2</sub> core/shell nanorods: Synthesis, structural and luminescent properties. *Luminescence* **2017**, *33*, 112–118. [[CrossRef](#)] [[PubMed](#)]
21. Zhu, X.; Yang, K.; Wu, A.; Bai, H.; Bao, J.; Qiao, Y.; Yang, Y.; Li, W.; Liu, Y. Luminescence studies and Judd–Ofelt analysis on SiO<sub>2</sub>@LaPO<sub>4</sub>:Eu@SiO<sub>2</sub> submicro-spheres with different size of intermediate shells. *Sci. Rep.* **2019**, *9*, 13065. [[CrossRef](#)]
22. Deng, T.; Zhang, Q. Optimization of LaPO<sub>4</sub>:Bi<sup>3+</sup> single-phased white-emitting phosphor luminescence properties by Li<sup>+</sup>/Na<sup>+</sup> doping. *Int. J. Opt.* **2019**, *2019*, 6. [[CrossRef](#)]
23. Dolgov, L.; Hong, J.-Y.; Zhou, L.; Li, X.; Li, J.; Đorđević, V.; Dramićanin, M.; Shi, J.; Wu, M. Efficient luminescence enhancement of Mg<sub>2</sub>TiO<sub>4</sub>:Mn<sup>4+</sup> red phosphor by incorporating plasmonic Ag@SiO<sub>2</sub> nanoparticles. *ACS Appl. Mater. Interfaces* **2019**, *11*, 21004–21009. [[CrossRef](#)]
24. Kushlyk, M.; Tsiumra, V.; Zhydashchuk, Y.; Haiduchok, V.; Syvorotka, I.I.; Sugak, D.; Suchocki, A. Enhancement of the YAG: Ce,Yb down-conversion emission by plasmon resonance in Ag nanoparticles. *J. Alloys Compd.* **2019**, *804*, 202–212. [[CrossRef](#)]
25. Jupri, S.A.; Ghoshal, S.K.; Yusof, N.N.; Omar, M.F.; Hamzah, K.; Krishnan, G. Influence of surface plasmon resonance of Ag nanoparticles on photoluminescence of Ho<sup>3+</sup> ions in magnesium-zinc-sulfophosphate glass system. *Opt. Laser Technol.* **2020**, *126*, 106134. [[CrossRef](#)]
26. Lina, L.; Yu, Z.; Wang, Z.; Zheng, B.; Feng, Z.; Zheng, Z. Plasmon-enhanced luminescence of Ag@SiO<sub>2</sub>/β-NaYF<sub>4</sub>:Tb<sup>3+</sup> nanocomposites via absorption & emission matching. *Mater. Chem. Phys.* **2018**, *220*, 278–285. [[CrossRef](#)]
27. Alkan, G.; Mancic, L.; Tamura, S.; Tomita, K.; Tan, Z.; Sun, F.; Rudolf, R.; Ohara, S.; Friedrich, B.; Milosevic, O. Plasmon enhanced luminescence in hierarchically structured Ag@(Y<sub>0.95</sub>Eu<sub>0.05</sub>)<sub>2</sub>O<sub>3</sub> nanocomposites synthesized by ultrasonic spray pyrolysis. *Adv. Powder Technol.* **2019**, *30*, 1409–1418. [[CrossRef](#)]
28. Lin, L.; Chen, J.; Wang, Z.; Feng, Z.; Huang, F.; Zheng, B.; Huang, L.; Yu, Z.; Zheng, Z. Plasmon-enhanced broad-band quantum-cutting of NaBaPO<sub>4</sub>:Eu<sup>2+</sup>, Yb<sup>3+</sup> phosphor decorated with Ag nano-particles. *Mater. Res. Bull.* **2017**, *93*, 35–41. [[CrossRef](#)]
29. Zheng, B.; Xu, S.; Lin, L.; Wang, Z.; Feng, Z.; Zheng, Z. Plasmon enhanced near-infrared quantum cutting of KYF<sub>4</sub>:Tb<sup>3+</sup>, Yb<sup>3+</sup> doped with Ag nanoparticles. *Opt. Lett.* **2015**, *40*, 2630–2633. [[CrossRef](#)] [[PubMed](#)]
30. Li, X.; Zhong, H.; Chen, B.; Sui, G.; Sun, J.; Xu, S.; Cheng, L.; Zhang, J. Highly stable and tunable white luminescence from Ag-Eu<sup>3+</sup> co-doped fluoroborate glass phosphors combined with violet LED. *Opt. Express* **2018**, *26*, 1870–1881. [[CrossRef](#)]
31. Amjad, R.J.; Dousti, M.R.; Sahar, M.R.; Shaukat, S.F.; Ghoshal, S.K.; Sazali, E.S.; Nawaz, F. Silver nanoparticles enhanced luminescence of Eu<sup>3+</sup> -doped tellurite glass. *J. Lumin.* **2014**, *154*, 316–321. [[CrossRef](#)]
32. Selvan, T.; Hayakawa, T.; Nogami, M. Remarkable influence of silver islands on the enhancement of fluorescence from Eu<sup>3+</sup> ion-doped silica gels. *J. Phys. Chem. B* **1999**, *103*, 7064–7067. [[CrossRef](#)]
33. Li, J.; Yang, Z.; Shao, B.; Liao, J.; Lai, S.; Qiu, J.; Song, Z.; Yang, Y. Ag nanoparticles-enhanced photoluminescence in LaPO<sub>4</sub>:Eu three-dimensional ordered macroporous films. *J. Am. Ceram. Soc.* **2015**, *98*, 1562–1566. [[CrossRef](#)]
34. Li, J.; Yang, Z.; Shao, B.; Yang, J.; Wang, Y.; Qiu, J.; Song, Z. Photoluminescence enhancement of SiO<sub>2</sub>-coated LaPO<sub>4</sub>:Eu<sup>3+</sup> inverse opals by surface plasmon resonance of Ag nanoparticles. *J. Am. Ceram. Soc.* **2016**, *99*, 3330–3335. [[CrossRef](#)]
35. Shannon, R.D. Revised effective ionic radii and systematic studies of interatomic distances in halides and chalcogenides. *Acta Cryst.* **1976**, *A32*, 751–767. [[CrossRef](#)]
36. Phadke, S.; Ninob, J.C.; Islam, M.S. Structural and defect properties of the LaPO<sub>4</sub> and LaP<sub>5</sub>O<sub>14</sub>-based proton conductors. *J. Mater. Chem.* **2012**, *22*, 25388–25394. [[CrossRef](#)]
37. Marciniak, L.; Strek, W.; Guyot, Y.; Hreniak, D.; Boulon, G. Synthesis and Nd<sup>3+</sup> luminescence properties of ALa<sub>1-x</sub>Nd<sub>x</sub>P<sub>4</sub>O<sub>12</sub> (A = Li, Na, K, Rb) tetraphosphate nanocrystals. *J. Phys. Chem. C* **2015**, *119*, 5160–5167. [[CrossRef](#)]
38. Wang, X.; Zhang, L.; Zhang, Z. Effects of pH value on growth morphology of LaPO<sub>4</sub> nanocrystals: Investigated from experiment and theoretical calculations. *Appl. Phys. A* **2016**, *122*, 7. [[CrossRef](#)]
39. Meyssamy, H.; Riwozki, K.; Kornowski, A.; Naused, S.; Haase, M. Wet-chemical synthesis of doped colloidal nanomaterials: Particles and fibers of LaPO<sub>4</sub>:Eu, LaPO<sub>4</sub>:Ce, and LaPO<sub>4</sub>:Ce,Tb. *Adv. Mater.* **1999**, *11*, 840–844. [[CrossRef](#)]

40. Vodnik, V.V.; Božanić, K.D.; Bibić, N.; Šaponjić, V.Z.; Nedeljković, M.J. Optical properties of shaped silver nanoparticles. *J. Nanosci. Nanotechnol.* **2008**, *8*, 3511–3515. [[CrossRef](#)]
41. Vukovic, V.V.; Nedeljkovic, M.J. Surface modification of nanometer-scale silver particles by imidazole. *Langmuir* **1993**, *9*, 980–983. [[CrossRef](#)]
42. Binnemans, K.; Goller-Walrand, C. Application of the Eu<sup>3+</sup> ion site symmetry determination. *J. Rare Earths* **1996**, *14*, 173–180.
43. Tanner, A.P. Some misconceptions concerning the electronic spectra of tri-positive europium and cerium. *Chem. Soc. Rev.* **2013**, *42*, 5090–5101. [[CrossRef](#)] [[PubMed](#)]
44. Quinten, M. The color of finely dispersed nanoparticles. *Appl. Phys. B* **2001**, *73*, 317–326. [[CrossRef](#)]



© 2020 by the authors. Licensee MDPI, Basel, Switzerland. This article is an open access article distributed under the terms and conditions of the Creative Commons Attribution (CC BY) license (<http://creativecommons.org/licenses/by/4.0/>).